


PAPER

[View Article Online](#)
[View Journal](#) | [View Issue](#)Cite this: *Nanoscale Adv.*, 2021, 3, 508

CdS decorated MnWO₄ nanorod nanoheterostructures: a new 0D–1D hybrid system for enhanced photocatalytic hydrogen production under natural sunlight†

Yogesh A. Sethi,^a Aniruddha K. Kulkarni,^b Anuradha A. Ambalkar,^a Supriya K. Khore,^a Aarti R. Gunjal,^a Suresh W. Gosavi^{*c} and Bharat B. Kale ^{*a}

Constructing a heterostructure is an effective strategy to reduce the electron–hole recombination rate, which enhances photocatalytic activity. Here, we report a facile hydrothermal method to grow CdS nanoparticles on MnWO₄ nanorods and their photocatalytic hydrogen generation under solar light. A structural study shows the decoration of hexagonal CdS nanoparticles on monoclinic MnWO₄. Morphological studies based on FE-TEM analysis confirm the sensitization of CdS nanoparticles (10 nm) on MnWO₄ nanorods of diameter-35 nm with mean length ~100 nm. The lower PL intensity of MnWO₄ was observed with an increasing amount of CdS nanoparticles, which shows inhibition of the charge carrier recombination rate. A CdS@MnWO₄ narrow band gap semiconductor was employed for photocatalytic hydrogen generation from water under solar light and the highest amount of hydrogen, *i.e.* 3218 $\mu\text{mol h}^{-1} \text{g}^{-1}$, is obtained which is 21 times higher than that with pristine MnWO₄. The enhanced photocatalytic activity is ascribed to the formation of a CdS@MnWO₄ nanoheterostructure resulting in efficient spatial separation of photogenerated electron–hole pairs due to vacancy defects. More significantly, direct Z-scheme electron transfer from MnWO₄ to CdS is responsible for the enhanced hydrogen evolution. This work signifies that a CdS decorated MnWO₄ nanoheterostructure has the potential to improve the solar to direct fuel conversion efficiency.

Received 10th October 2020
Accepted 8th December 2020

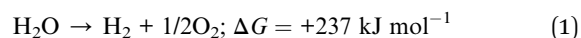
DOI: 10.1039/d0na00843e

rsc.li/nanoscale-advances

1. Introduction

Global energy consumption and rapid environmental pollution are serious societal concerns due to the massive use of fossil fuels such as coal, oil, and natural gas. Furthermore, the combustion of these fossil fuels causes serious environmental impacts ranging from air and water contamination to global warming. Therefore, it is high time to develop renewable clean carbon-free energy resources to control our dependence on fossil fuels.^{1,2} Hydrogen, which as a fuel has been attractive for the replacement of fossil fuels, could be an alternative energy source for solving the current energy crisis and environmental pollution. Hydrogen evolution from photocatalytic water splitting using semiconductors is one promising environmentally

friendly approach to solving our current and future energy portfolio. Photocatalytic water splitting as a process of decomposition of water (H₂O) using sunlight energy is an economical approach to converting solar energy into chemical energy (H₂) and oxygen (O₂) fuel for storage.^{3,4}



The key factors for effective photocatalysts are high visible light activity, inexpensiveness, and long-term stability. Pioneering work was done by Fujishima and Honda using TiO₂ electrodes.⁵ In the last four decades, various semiconductors have been designed and developed for photocatalytic hydrogen generation, such as ZnO,⁶ Cu₂O,⁷ Nb₂O₅,⁸ Ta₂O₅,⁹ WO₃,¹⁰ CdS,¹¹ and ZnS.¹² However, binary oxide/sulfide photocatalysts have low photocatalytic efficiency due to their high resistance, unsuitable band gap, low stability, rapid electron–hole pair recombination, and photo-corrosion.^{13,14} Previous reports have shown that cation/anion doping in metal oxides and noble metal loading (Ag, Au, Pt, *etc.*) on TiO₂ potentially tune the band gap and enhance absorption towards the longer wavelength. Nevertheless, the expected outcome in the activity of the photocatalyst is unremarkable because of its poor efficiency and

^aNanocrystalline Laboratory, Centre for Material for Electronic Technology (CMET), Department of Information Technology, Govt. of India, Panchawati, Off Pashan Road, Pune 411007, India. E-mail: bbkale1@gmail.com; bbkale@cmet.gov.in; Fax: +91 20 2589 8180; Tel: +91 20 2589 9273

^bProf. John Barnabas School for Biological Studies, Department of Chemistry, Ahmednagar College, Ahmednagar, India, 414001

^cDepartment of Physics, Savitribai Phule Pune University, Pune, India, 411008

† Electronic supplementary information (ESI) available. See DOI: 10.1039/d0na00843e

mixed side products.^{15,16} Therefore, the development of an active semiconductor photocatalyst is still a great challenge for the scientific community. Recently, transition metal tungstates of the type (MWO₄) (M = CO, Ni, Cu, or Zn, *etc.*) have attracted widespread interest as promising candidates owing to their high stability, low cost, and unique crystal structure, and these compounds have a broad range of applications.^{17,18} Among different tungstates, the wolframite-type monoclinic structure of manganese tungstate (MnWO₄) is a very promising material due to its suitable bandgap of 2.7 eV, which can effectively absorb visible light, relatively high stability, excellent reactivity, *etc.*¹⁹ However, its photocatalytic performance is very low due to limited light absorption in the visible region.²⁰ Recently, many efforts have been made to use MnWO₄ for the photocatalytic decomposition of organic pollutants and hydrogen generation. However, the photocatalytic activity of pure MnWO₄ is still poor due to the quick recombination of photogenerated electron and hole pairs. Moreover, electrons in the conduction band (CB) of MnWO₄ (+0.4 eV NHE) cannot reduce O₂ *via* single-electron processes, which greatly limits the photocatalytic performance of MnWO₄.^{21,22} Therefore, the photocatalytic activity of MnWO₄ needs to be further improved for use in practical applications. In the past, immense work has been done in the synthesis of heterojunctions wherein one photocatalyst coupled with another catalyst is significantly beneficial to enhancing photocatalytic activities.^{23,24} Therefore, coupling MnWO₄ with another co-catalyst with matching bandgap is an ideal way to enhance the photocatalytic activity of MnWO₄. Among different co-catalysts, cadmium sulfide (CdS) has attracted a lot of attention for the construction of a heterojunction due to its narrow bandgap with a high CB position, which can greatly enhance the photocatalytic activity by effectively separating the electron-hole pairs, and its visible light absorption.²⁵ Many CdS-based heterojunction photocatalysts have been developed so far, including CdS/WO₃,²⁶ MoS₂/CdS,²⁷ CdS/ZnWO₄,²⁸ and CdS/BiVO₄,²⁹ which were prepared *via* different methods and showed enhanced photocatalytic activities. We have also reported CdS@CdWO₄,³⁰ for hydrogen generation and pollutant degradation. These hybrid multi-semiconductor Z-scheme systems have advantages with one semiconductor having a high CB minimum and the other a low VB maximum and therefore they can provide a large overpotential for the photocatalytic process and also reduce charge carrier recombination. Therefore, the formation of a CdS@MnWO₄ heterojunction can create an ideal photocatalyst for photocatalytic hydrogen evolution. Herein, we report a successful synthesis of a CdS@MnWO₄ heterostructure photocatalyst with different molar ratios through a facile hydrothermal method. Similarly, the as-prepared photocatalyst was subjected to a photocatalytic water splitting reaction for hydrogen generation under visible light irradiation and it shows a much-improved hydrogen generation rate compared to pure photocatalysts. In the present work, we have successfully synthesized a highly efficient CdS@ZnWO₄ heterostructure photocatalyst using the hydrothermal method, in which CdS nanoparticles are decorated on 1D MnWO₄ nanorods. To the best of our knowledge, this is the first report on CdS/MnWO₄ to describe enhanced photocatalytic activity *via* Z-scheme electron

transfer for hydrogen generation under solar light. In this work, the effect of CdS on the structural, optical, morphological and photocatalytic properties was investigated and is discussed. The Z-scheme mechanism of photocatalytic hydrogen from water is also proposed.

2. Experimental sections

Sodium tungsten oxide di-hydrates (Na₂WO₄·2H₂O), manganese nitrate tetra-hydrate (Mn(NO₃)₂·4H₂O), cadmium nitrate tetrahydrate (Cd(NO₃)₂·4H₂O), and thiourea (NH₂CSNH₂) used for the preparation of the catalyst were of analytical grade (SD Fine-Chem Limited, India) and used without any further purification.

2.1 Synthesis of MnWO₄ and CdS@MnWO₄ nanorods

In a typical synthesis, 0.05 mol of Na₂WO₄·2H₂O and 0.05 mol of Mn(NO₃)₂·4H₂O were dissolved in 140 mL of distilled water and stirred for 20 min. The clear solution was then transferred into a 200 mL capacity Teflon autoclave and kept at 180 °C for 24 h. After the completion of the reaction, the autoclave was cooled naturally. After washing several times with absolute ethanol and deionized water, a brownish colored powder was obtained. This pure sample is labeled MNW-0. Similarly, CdS@MnWO₄ composites have been synthesized by following the same route with the addition of 5, 10, 15, 20 M% of cadmium nitrate (Cd(NO₃)₂·4H₂O) and thiourea (TU) to the above solution. These samples have been labeled MNC-1, 2, 3, and 4.

2.2 Photocatalytic study

2.2.1 Photocatalytic hydrogen generation from water.

Photocatalytic hydrogen generation was carried out through water splitting at room temperature under sunlight with 0.1 g of each photocatalyst sample suspended in 100 mL of double distilled water and Na₂S/Na₂S₂O₃ as a sacrificial reagent in the reactor system. Pure MnWO₄ and MNW photocatalysts were added with 0.5 wt% preloaded platinum as a co-catalyst. Argon gas was purged through this reaction mixture to remove the dissolved gases. The 250 mL round bottom flask was connected to a graduated measuring gas collector tube. The gas collector tube had a septum arrangement to get rid of the evolved gas through a gas-tight syringe and to measure the amount of gas evolved. The amount of gas evolved was noted over time. The purity of the collected gas was analyzed using gas chromatography (Model Shimadzu GC-14B, MS-5 Å column, TCD, Ar carrier).

2.2 Sample characterization

The as-synthesized powders were analyzed to determine their phase purity and crystalline structure by using the X-ray diffraction (XRD) technique (Advance, Bruker AXS D8) using Cu Kα1 (1.5406 Å) radiation. The bandgap of the samples was determined by using a UV-VIS spectrophotometer (Perkin-Elmer) in the range of 300–800 nm. Morphological studies and crystallinity analysis were carried out using high-resolution



transmission electron microscopy (HRTEM Philips EM-CM-12) operated at an accelerating voltage of 200 kV. The photoluminescence (PL) spectra were recorded using an F-3 fluorescence spectrophotometer (Horiba Jobin Yvon).

3. Results and discussions

3.1 Structural study

The crystal structure and phase formation of the as-synthesized MnWO_4 (MNW-0) and CdS@MnWO_4 nanocomposites (MNC-1, 2, 3, and 4) were determined by powder XRD (Fig. 1). Fig. 1 shows well-indexed diffraction peaks of MNW-0, indicating single-phase formation of a MnWO_4 monoclinic structure of wolframite-type, matching the reported values (JCPDS card no 015-0774). All the reflection peaks were indexed with lattice parameters $a = 4.80 \text{ \AA}$, $b = 5.71 \text{ \AA}$, $c = 4.97 \text{ \AA}$ and $\beta = 91.22^\circ$ (space group $P2_1/c$, with $Z = 2$). In the case of CdS@MnWO_4 composites (MNW-1–4), small additional peaks are observed with the co-existence of both MNW and CdS phases without any trace of other impurities, demonstrating the successful formation of the CdS@MnWO_4 composite material. The three main diffraction peaks are located at $2\theta = 24.79^\circ$, 26.42° , and 28.22° , corresponding to crystal diffraction planes of $(1\ 0\ 0)$, $(0\ 0\ 2)$, and $(1\ 0\ 1)$, respectively, of the hexagonal phase of CdS, matching well with JCPDS card no 06-0314, and labeled by vertical red dashed lines in Fig. 1. Furthermore, the intensity of the CdS peaks is less sharp than that of MNW, due to the lower concentration of CdS compared to pure MnWO_4 . Furthermore, the intensity of the CdS peaks increases as the CdS concentration increases.³¹ Overall, the CdS@MnWO_4 samples with different CdS amounts show slight declines in the peaks observed in sample MNC-4 at 29.9 , 36.04 , 40.02° . The decrease in peak intensity of MnWO_4 is due to its low crystallization due to higher CdS content, which suppresses the growth of MnWO_4

in the MNC-4 sample. The XRD result suggests that the CdS nanoparticles were probably decorated on the surface of MnWO_4 and were not incorporated into the lattice of MnWO_4 .

3.2 Surface and morphological studies

Transmission electron microscope (TEM) and high-resolution transmission electron microscope (HR-TEM) analyses were performed to further investigate the morphology and hetero-junction formation of the as-prepared samples. Fig. 2 shows the comparative TEM and HRTEM images of the MnWO_4 and CdS@MnWO_4 samples. Fig. 2a shows the TEM image of pure MnWO_4 , in which nanoparticles are gathered with a large number of particles forming nanorods. The length of nanorods in the range of approximately 100–150 nm and diameter around 30–35 nm. The HRTEM image (Fig. 2b) shows lattice fringes of the material with an interplanar distance with a calculated d spacing (0.4813 nm) matching well with the d spacing of the $(1\ 0\ 0)$ plane of the MnWO_4 monoclinic cell. A selected area diffraction (SAED) pattern (inset to Fig. 2a) shows bright spots in the line pattern, confirming that the MnWO_4 nanorods are single crystalline in nature. Fig. 2c and d shows the TEM and HRTEM images of CdS@MnWO_4 , respectively. As can be seen from Fig. 2c and d by comparison with pure MnWO_4 , the CdS-loaded samples show almost the same nanorods as MnWO_4 with the addition of spherical nanoparticles. The spherical nanoparticles of CdS with a size of 10–15 nm were uniformly anchored on the surface of MnWO_4 nanorods, which demonstrates the successful formation of a CdS@MnWO_4 hetero-junction. Furthermore, the HR-TEM images (Fig. 2d) of CdS@MnWO_4 also show two distinct sets of lattice fringes with different orientations. The parallel lattice fringes with interplanar spacings of 0.362 nm and 0.360 nm correspond to the $(1\ 1\ 0)$ and (100) crystallographic planes of monoclinic MnWO_4 and hexagonal CdS, respectively. The inset to Fig. 2c represents

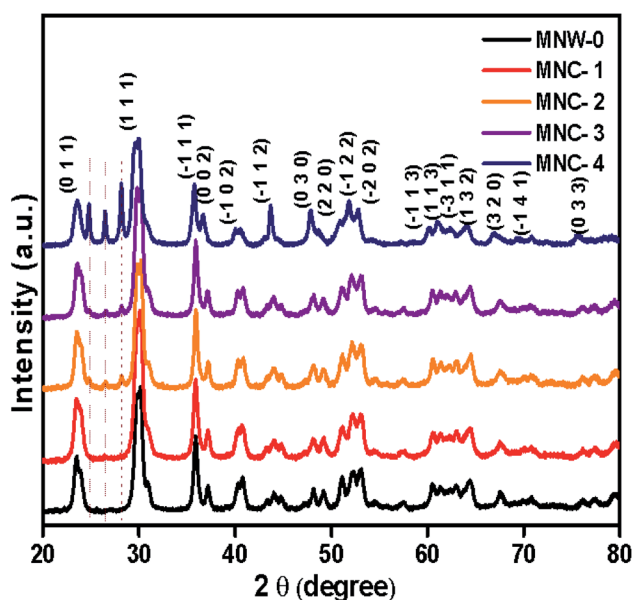


Fig. 1 X-ray diffraction patterns of MnWO_4 (MNW-0) and CdS@MnWO_4 (MNC-1–4).

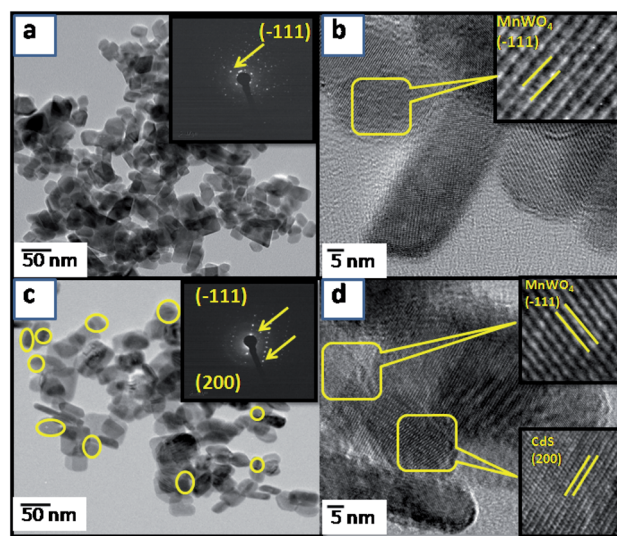
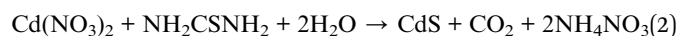


Fig. 2 FE-TEM images of pure MnWO_4 (a, b) and (c, d) CdS@MnWO_4 nanorods (MNC-3). The inset shows the corresponding SAED pattern.

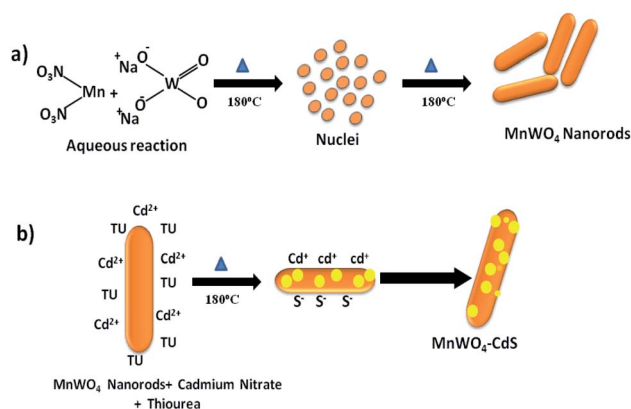
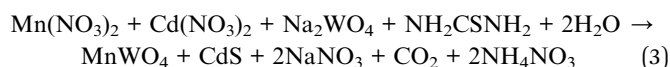


the SAED image of the sample, which confirms the single-crystalline nature of MnWO_4 .

To study the growth kinetics of morphology (more specifically the nucleation process, crystal growth, and Ostwald's ripening process), we employed water as a reaction medium at 180 °C temperature. After the evaluation of the morphological features of as-synthesized CdS@MnWO_4 nanoheterostructures, we have proposed a growth mechanism for the formation of nanoheterostructures. It is well known that two main parameters affect the growth of a crystal: *i.e.* temperature and the supersaturation of the solution. A highly supersaturated solution was obtained to study during the crystallization where amorphous fine particles act as precursors under hydrothermal conditions at 180 °C. This growth process is called the Ostwald ripening process. At the beginning of the reaction, nucleation takes place in a supersaturated solution; then there is the formation of small nanoparticles. These nanoparticles self-align and form nanorods. In a solvothermal reaction, MnWO_4 nanorods with a length of 150 nm and width of 50 nm are formed at the expense of the self-alignment of MnWO_4 nanoparticles with prolonged reaction time (Scheme 1). The TEM images also suggest that nanorods grow in the direction of the (1 1 0) plane at the expense of smaller nanoparticles, as discussed above. When the growth of MnWO_4 nanoparticles is allowed in the presence of cadmium nitrate and thiourea, the CdS nanoparticles are grown on the surfaces of the MnWO_4 nanorods. Cadmium nitrate ($\text{Cd}(\text{NO}_3)_2 \cdot 6\text{H}_2\text{O}$) and thiourea ($\text{CH}_4\text{N}_2\text{S}$) react under the hydrothermal conditions and form $\text{H}_2\text{NCCdSNH}_2$ + aqueous chelate which further decomposes and forms CdS@MnWO_4 composite nanostructures.²⁷ The possible reactions for the formation of a CdS@MnWO_4 heterostructure are as follows:³²



Overall reaction:



Scheme 1 Formation of the growth mechanism of MnWO_4 nanorods and CdS@MnWO_4 nanorods.

Initially, MnWO_4 formation takes place and after the saturation of MnWO_4 , CdS formation takes place on the surface of the MnWO_4 nanorods *via* reaction (2).

Scheme 1 shows the formation of MnWO_4 nanorods and the anchoring of CdS nanoparticles on the surface of MnWO_4 . Under hydrothermal conditions, the Mn^{2+} and WO_4^{2-} ions react with each other and form MnWO_4 nanoparticles. Furthermore, due to prolonged hydrothermal treatment, the nanoparticles self-align in one direction and form nanorods as per the crystal growth phenomenon (Ostwald ripening) as discussed above (Scheme 1a). Furthermore, MnWO_4 nanorods become saturated with Cd^{2+} and S^{2-} ions (Scheme 1b) and form CdS nanoparticles on the surface under hydrothermal conditions.

3.3 Optical properties

The optical properties of the as-synthesized material were examined by UV-visible diffused absorption spectra. Fig. 3 shows the comparative UV DRS spectra for pure MnWO_4 nanorods (MNC-0) and different concentrations of CdS@MnWO_4 (MNC-1, 2, 3, and 4) nanoheterostructures. Fig. 3 reveals that the absorption edges of pure MnWO_4 (MNC-0) show two edges at approximately 455 nm and 575 nm, respectively. In the case of MnWO_4 , weak absorption at 575 nm is due to the d^5 electronic configuration of Mn(II) causing a $d-d$ electronic transition which is spin forbidden; therefore it shows a weak absorption peak at 575 nm.³³ In comparison to pure MnWO_4 , the absorption edges of the CdS@MnWO_4 samples were gradually red-shifted with increasing CdS content. The following formula can be used to calculate the band gap energy for one semiconductor: $\alpha h\nu = A(h\nu - E_g)^{n/2}$ where $h\nu$, α , A , and E_g are the light energy, absorption energy, constant value, and the band gap of the semiconductor and n is the transition type of the semiconductor: $n = 1$ for a direct transition and $n = 4$ for an indirect transition. The calculated band gaps for MnWO_4 and CdS were 2.74 and 2.34 eV. With an increase in CdS the band gap of CdS@MnWO_4 is closer to that of CdS (ESI I Table 1†).

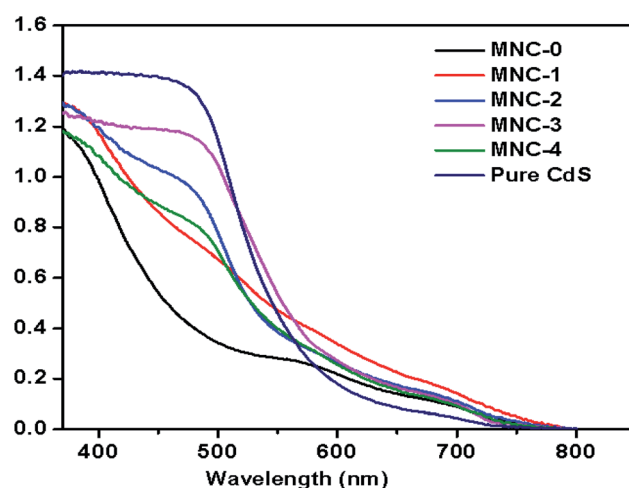


Fig. 3 UV-Vis absorption spectra of pure MnWO_4 (MNC-0) and CdS@MnWO_4 prepared using different concentrations of CdS (MNC-1 to 4).



Table 1 The H₂ generation rates for as-synthesized MnWO₄ nanorods (MNW-0) CdS@ZnWO₄ and pure CdS prepared using different concentrations of cadmium nitrate (MNC-1–4)

Sr. no.	Sample	H ₂ evolution rate (μmol h ⁻¹ g ⁻¹)
1	MNW-0	153
2	MNC-1	916
3	MNC-2	1368
4	MNC-3	3218
5	MNC-4	2479
6	Pure CdS	380

This indicates that coupling with CdS could narrow the band gap value of MnWO₄, thus leading to improved optical absorption in the visible light region (Table 1).

Photoluminescence spectra (PL) were performed to study different energy states available between the VB and the CB which are responsible for radiative recombination. Fig. 4 shows comparative room-temperature PL spectra of as-synthesized pure and CdS@MnWO₄ excited at a wavelength of 325 nm. Pure MnWO₄ shows a broad emission peak in the wavelength range 525–530 nm, well matching previous reports. The PL emission spectra for pure MnWO₄ show bands at wavelengths of 416, 452, 470, 497, 482, and 576 nm, attributed to the transition from the 1A1 ground state to the high vibration level of 1T2 and from the low vibration level of 1T2 to the 1A1 ground state within tetragonal WO₄²⁻ groups. The PL spectra for MNC-1, 2, 3 and 4 show two strong emission peaks centered at wavelengths of 468, and 530–540 nm that can be assigned to CdS and MnWO₄, and peaks contributing to the band-to-band PL phenomenon with the energy of light equal to the band gap energy.^{34,35} The peak observed at wavelength 530–540 nm is assigned to the trapped electron-hole pairs or excitations bound to ionized donors and shows an intrinsic character with surface defects due to CdS.³⁶ From the PL

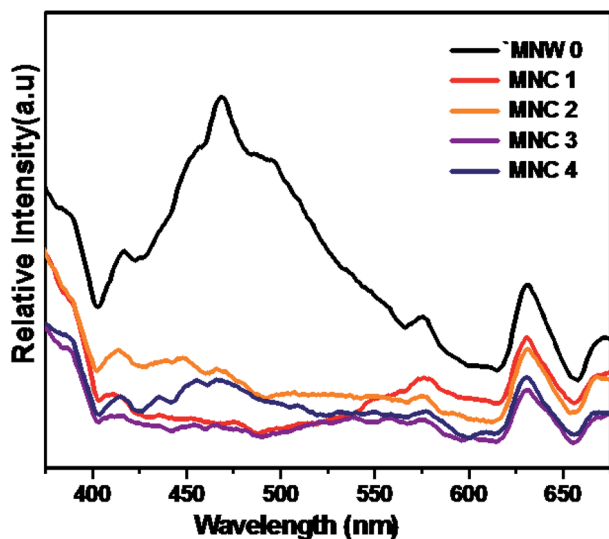


Fig. 4 Photoluminescence spectra of CdS@MnWO₄: (a) MNW-0 (black), (b) MNC-1 (red), (c) MNC-2 (orange), (d) MNC-3 (purple) and (e) MNC-4 (blue).

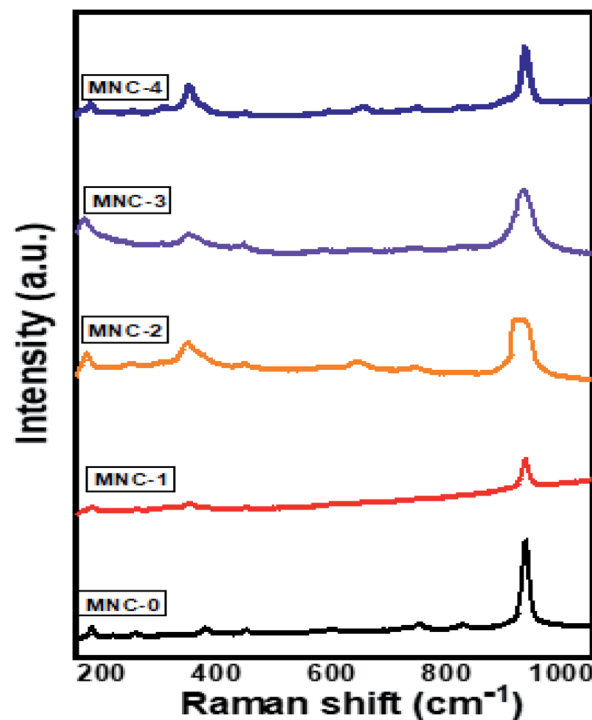


Fig. 5 Raman shifts of pure MNW-0 and MNC-1–4.

spectra it is clear that with an increase in the concentration of CdS on MnWO₄ a redshift in the peak at 530 nm is observed, due to an increase in the concentration of CdS nanoparticles.³⁷ From Fig. 4 it can also be observed that with an increase in CdS loading on MnWO₄ nanorods, the PL intensity decreases, suggesting a lower electron-hole pair recombination rate due to the presence of surface defects.^{35,36} The above results show that surface modification by CdS on MnWO₄ drastically decreased the PL intensity.

Samples MNW-0 and MNW-3 were employed for Raman analysis and the corresponding data is shown in Fig. 5. All the peaks were observed in the range 500–1200 cm⁻¹ at room temperature. Pure MnWO₄ shows a strong intense band observed at 885.3 cm⁻¹ corresponding to Ag modes originating from the symmetric stretching vibration of a short terminal W–O bond, while the asymmetric stretching vibration from the W–O bond is located at 774 cm⁻¹ corresponding to B_g modes. Some weak bands contribute to asymmetric stretching vibration modes of longer W–O bonds, at 696, 516, 548 cm⁻¹, deformation vibration of short W–O bond in (W₂O₄)_n chains, and 330 and 397 cm⁻¹ vibration modes of Mn–O bonds.^{38–40} The sample MNC shows broad peaks at 297, 592, and 882 cm⁻¹ associated with CdS. All three peaks are assigned to the first overtone mode (LO), second overtone mode (2LO) and third overtone mode (3LO) of CdS, respectively.⁴¹ Samples MNC-1–4 show the presence of both CdS and MnWO₄, providing clear evidence for the formation of a CdS@MnWO₄ heterojunction.

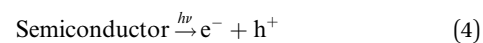
3.4 Photocatalytic study

3.4.1 Photocatalytic H₂ evolution from H₂O splitting. Photocatalytic H₂ generation was studied with a water-splitting

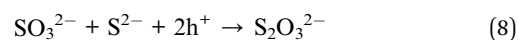
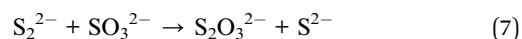
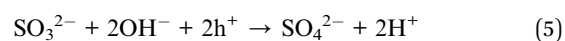


reaction using $\text{Na}_2\text{S}/\text{Na}_2\text{S}_2\text{O}_3$ solution under solar light irradiation in which $\text{Na}_2\text{S}/\text{Na}_2\text{S}_2\text{O}_3$ acts as a sacrificial agent.⁴² Hydrogen measurement was performed under solar light at room temperature and the amount of hydrogen was determined by gas chromatography (GC). No hydrogen gas was detected in the absence of a photocatalyst or in the dark, indicating that hydrogen is due to the presence of light with a semiconductor photocatalyst. For the hydrogen generation experiment, we used 70 mL of DI water, and a mixture of 0.25 M Na_2S and 0.35 M $\text{Na}_2\text{S}_2\text{O}_3$ was used as a sacrificial agent. The role of a sacrificial agent is not only to resist photocorrosion but to oxidize S_2^{2-} into S^{2-} , which supports the enhancement of free electrons. Previous reports show the detailed mechanism of the water splitting reaction in which the semiconductor absorbs solar light equal to or greater than the band gap energy, generating electrons in the CB and holes in the VB. The redox reaction takes place on the surface of the semiconductors with adsorbed species. The photogenerated holes from the VB irreversibly oxidize S_2^{2-} , which is reduced back to S^{2-} by $\text{Na}_2\text{S}_2\text{O}_3$ and is instantaneously adsorbed on the semiconductor surface, producing protons (H^+) and free radicals, while electrons from the CB reduce H^+ ions into molecular hydrogen H_2 .⁴³ Fig. 6 shows the time-dependent H_2 evolution rates of all as-synthesized materials, indicating that MnWO_4 NRs and CdS alone produced relatively very low amounts of hydrogen, *i.e.* $153 \mu\text{mol h}^{-1} \text{g}^{-1}$ and $380 \mu\text{mol h}^{-1} \text{g}^{-1}$ (ESI II†), but CdS@MnWO_4 exhibits $3218 \mu\text{mol h}^{-1} \text{g}^{-1}$, which is 21 times higher than MnWO_4 . Scheme 2 shows that after the decoration of CdS nanoparticles on MnWO_4 , there is enhanced photocatalytic activity. The rate of hydrogen production increases with the amount of CdS content. The maximum hydrogen production of $3218 \mu\text{mol h}^{-1} \text{g}^{-1}$ was obtained for sample MNC-3 CdS decorated MnWO_4 . Furthermore, it is observed that with an increase in CdS to 20% (MNC-4) CdS@MnWO_4 the rate of hydrogen production decreases to $2479 \mu\text{mol h}^{-1} \text{g}^{-1}$. The decrease in photocatalytic activity for MNC compared with MNC-3 is due to rapid electron-hole pair recombination and a shielding effect

towards light absorption due to excess CdS decoration. Furthermore, the PL study also supports the finding that the lower the PL intensity, the higher the separation rate of photo-induced charges, and, possibly, the higher the photocatalytic activity. Sample MNC-3 shows lower PL intensity compared to MNC-4, a higher separation rate of photoinduced charges, and, possibly, higher photocatalytic activity. Historically, CdS-decorated nanomaterial heterostructures exhibited enhanced photocatalytic activity towards hydrogen generation and effective charge carrier separation. For example Chava *et al.*⁴⁴ reported 1D-0D CdS-SnS₂ nanorods for excellent photocatalytic hydrogen evolution activity. Similarly, Shandong *et al.*⁴⁵ prepared a CdS/NiS hybrid photocatalyst where NiS acts as a co-catalyst which exhibits maximum hydrogen evolution (with $793.6 \mu\text{mol h}^{-1}$). The enhanced photocatalytic activity was due to intimate contact between CdS/NiS reducing the electron-hole pair recombination rate. In that direction recently, we have reported CdS-decorated CdWO_4 nanorods for hydrogen generation and efficient dye degradation.³⁰ The above results show that CdS-based semiconductor heterostructures effectively enhance stability and photocatalytic activity. Similarly, in the present work with CdS nanoparticles decorated on MnWO_4 nanorods, the advantage of CdS is its ability to harvest solar light.²¹ In addition, the heterojunction between CdS@MnWO_4 inhibits the electron-hole pair recombination rate, thereby enhancing photocatalytic activity. Furthermore, the MnWO_4 nanorods provide space to protect CdS from the photocorrosion problem. Hence, the optimum quantity of CdS on MnWO_4 enhances photocatalytic hydrogen generation under solar light. Furthermore, a recycling study shows stable hydrogen evolution under solar light (ESI: III Table 2†).



Oxidation:



Reduction:

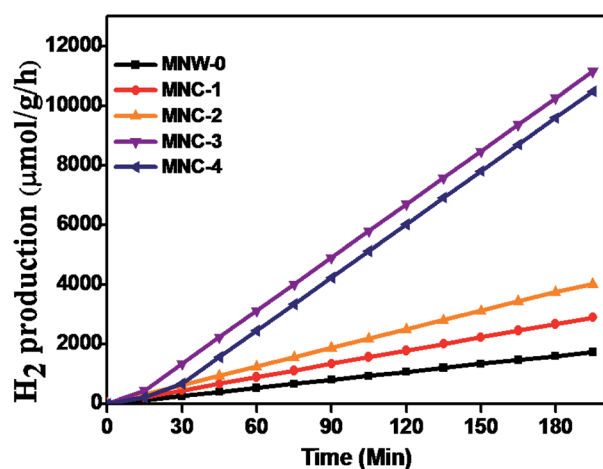


Fig. 6 Photocatalytic hydrogen generation via H_2O splitting with CdS@MnWO_4 : (a) MNW-0 (black), (b) MNC-1 (red), (c) MNC-2 (orange), (d) MNC-3 (purple) and (e) MNC-4 (blue).

3.4.2 Possible mechanism of photocatalytic activity using CdS@MnWO_4 . The Z-scheme photocatalytic mechanism of the CdS@MnWO_4 nanoheterostructure is proposed and discussed. It has been well reported that the photocatalytic activity of a semiconductor depends on the optical band gap, crystal structure, electron-hole pair recombination rate, *etc.* However, photocatalytic activity depends specifically on band structure:

i.e. the position of the bottom of the VB and the top of the CB of both MnWO_4 and CdS . The valence band and conduction band potentials of MnWO_4 and CdS can be calculated using the following equations:

$$E_{\text{VB}} = \chi - E_{\text{fe}} + \frac{1}{2}E_{\text{g}} \quad (10)$$

$$E_{\text{CB}} = \chi - E_{\text{fe}} - \frac{1}{2}E_{\text{g}} \quad (11)$$

where E_{VB} and E_{CB} are the valence band and conduction band edge potentials, respectively, χ is the electronegativity of the semiconductor, which is the geometric mean of the electronegativity of the constituent atoms. E_{fe} is the energy of free electrons on the hydrogen scale (about -4.5 eV) and E_{g} is the band gap energy of the semiconductor. As per the literature, the values of χ for MnWO_4 and CdS have been calculated as 6.12 eV and 5.04 eV, respectively.⁴⁶ Based on band gap positions, the band edge potentials of the VB and CB for MnWO_4 are 2.95 and 0.27 eV while for CdS they are 2.18 and -0.12 eV, respectively.²³ Based on the above values, a possible mechanism is illustrated in Scheme 2. In the presence of solar light, CdS and MnWO_4 with their band gaps of 2.3 and 2.68 eV, respectively, undergo photoexcitation.²³ However, pure MnWO_4 shows poor photocatalytic activity due to its wide band gap compared with CdS . In the present case, a CdS@MnWO_4 photocatalytic mechanism is proposed *via* a Z-scheme, as shown in Scheme 2. As illustrated in Scheme 2 under visible light both CdS and MnWO_4 are excited and generate photoinduced electron-hole pairs. The electrons from CdS transfer to MnWO_4 *via* strong intimate contact through the interface due to the more negative Fermi level of CdS , leaving holes on the CdS . Due to the transfer of electrons from the CB of CdS which have the energy to stride over the potential barrier, they can be transported from CdS to MnWO_4 . Therefore, the existence of a potential barrier goes against the transmission of photoinduced electrons from the CB of CdS to the CB of MnWO_4 . The same principle can be applied to the transfer of photoinduced holes from the VB of MnWO_4 to the CB of CdS . In construction, the band structure is

more suitable to transfer photogenerated electrons from the CB of MnWO_4 to the VB of CdS : *i.e.* electrons migrate from the CB of CdS to the VB of MnWO_4 through the Z direction.⁴⁶ This migration process leaves the photoexcited electrons in the CB of CdS and photoexcited holes in the VB of MnWO_4 . The electrons from the CB of CdS possess a strong reducibility ability which can drive hydrogen generation. This enhancement occurs due to the Z-scheme heterostructure, which facilitates an effective electron-hole pair separation and also enhances the redox ability of a photocatalyst.⁴⁷ Hence, the Z-scheme mechanism enhances the recombination of the electron-hole pair in the case of CdS@MnWO_4 .

4. Conclusions

In summary, hierarchical CdS nanoparticles have been decorated on the surface of MnWO_4 architectures that have been constructed *via* an *in situ* hydrothermal method. The structural, optical, and morphological properties of as-prepared CdS@MnWO_4 with varied amounts of CdS were studied systematically. FE-TEM analysis showed the existence of a heterojunction between CdS and MnWO_4 nanorods, and the effect of CdS decoration on MnWO_4 was investigated by a photoluminescence study. In the case of CdS@MnWO_4 , CdS acts as a sensitizer for MnWO_4 to capture sunlight and also acts as a co-catalyst to promote the electron-hole pair separation rate under solar light irradiation. The heterojunction between CdS@MnWO_4 exhibits excellent photocatalytic H_2 evolution *via* H_2O splitting under natural sunlight. The encouraging results presented in this work demonstrate the potential of CdS@MnWO_4 as an active photocatalyst for hydrogen evolution from water.

Conflicts of interest

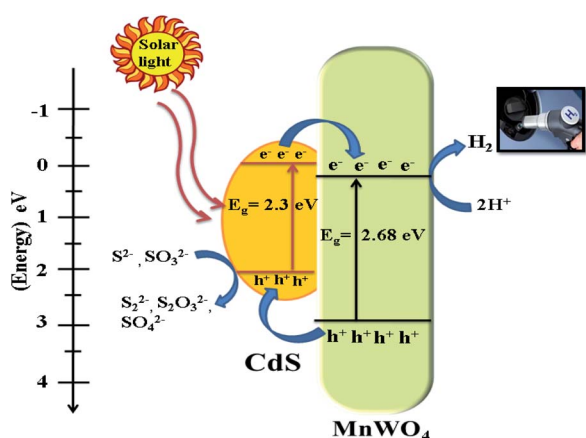
There are no conflicts to declare.

Acknowledgements

BBK & YAS would like to thank the Ministry of Electronics and Information Technology (MeitY), the Government of India for financial support, and C-MET Pune for providing research facilities. AKK would like to thank ASPIRE SPPU for financial support under the project scheme. SWG would like to thank SPPU, Physics Department for technical support. The authors would like to thank the Nanocrystalline materials group for kind support.

References

- 1 X. Chen, C. Li, M. Gratzel, K. Robert and S. S. Mao, Nanomaterials for renewable energy production and storage, *Chem. Soc. Rev.*, 2012, **41**, 7909.
- 2 L. Jing, W. Zhou, G. Tian and H. Fu, Surface tuning for oxide-based nanomaterials as efficient photocatalysts, *Chem. Soc. Rev.*, 2013, **42**, 9509.



Scheme 2 Schematic representation of photocatalytic hydrogen generation using CdS@MnWO_4 .



- 3 F. E. Osterloh, Inorganic materials as catalysts for photochemical splitting of water, *Chem. Mater.*, 2008, **20**, 35–54.
- 4 J. Ran, J. Zhang, J. Yu, M. Jaroniec and S. Z. Qiao, Earth-abundant cocatalysts for semiconductor-based photocatalytic water splitting, *Chem. Soc. Rev.*, 2013, 1–26.
- 5 A. Fujishima and K. Honda, Electrochemical Photolysis of Water at a Semiconductor Electrode, *Nature*, 1972, **238**, 37.
- 6 F. Liao, Z. Zeng, C. Eley, Q. Lu, X. Hong and S. C. E. Tsang, Electronic Modulation of a Copper/Zinc Oxide Catalyst by a Heterojunction for Selective Hydrogenation of Carbon Dioxide to Methanol, *Angew. Chem., Int. Ed.*, 2012, **51**, 5832.
- 7 Y.-F. Zhao, Z.-Y. Yang, Y.-X. Zhang, L. Jing, X. Guo, Z. Ke, P. Hu, G. Wang, Y.-M. Yan and K.-N. Sun, Cu₂O Decorated with Cocatalyst MoS₂ for Solar Hydrogen Production with Enhanced Efficiency under Visible Light, *J. Phys. Chem. C*, 2014, **118**(26), 14238–14245.
- 8 A. K. Kulkarni, R. P. Panmand, Y. A. Sethi, S. R. Kadam, S. P. Tekale, G.-H. Baeg, A. V. Ghule and B. B. Kale, In situ preparation of N doped orthorhombic Nb₂O₅ nanoplates/rGO composites for photocatalytic hydrogen generation under sunlight, *Int. J. Hydrogen Energy*, 2018, **43**, 19873.
- 9 A. Kohlsdorf, D. H. Taffa and M. Wark, Microwave assisted synthesis of Ta₂O₅ nanostructures for photocatalytic hydrogen production, *J. Photochem. Photobiol.*, 2018, **366**, 41–47.
- 10 X. Chen, Y. Zhou, Q. Liu, Z. Li, J. Liu and Z. Zou, Ultrathin, Single-Crystal WO₃ Nanosheets by Two-Dimensional Oriented Attachment toward Enhanced Photocatalytic Reduction of CO₂ into Hydrocarbon Fuels, *ACS Appl. Mater. Interfaces*, 2012, **4**, 3372.
- 11 Y.-J. Yuan, D. Chen, Z.-T. Yu and Z.-G. Zou, Cadmium sulfide-based nanomaterials for photocatalytic hydrogen production, *J. Mater. Chem. A*, 2018, **6**, 11606–11630.
- 12 S. K. Apte, S. N. Garje, S. S. Arbuj, B. B. Kale, J. O. Baeg, U. P. Mulik, S. D. Naik, D. P. Amalnerkar and S. W. Gosavi, A novel template free, one pot large scale synthesis of cubic zinc sulfide nanotriangles and its functionality as an efficient photocatalyst for hydrogen production and dye degradation, *J. Mater. Chem.*, 2011, **21**, 19241–19248.
- 13 S. Chen, D. Huang, P. Xu, W. Xue, L. Lei, M. Cheng, R. Wang, X. Liu and R. Deng, The effect of the photochemical environment on photoanodes for photoelectrochemical water splitting, *J. Mater. Chem. A*, 2020, **8**, 2286–2322.
- 14 N. Fajrina and M. Tahir, A critical review in strategies to improve photocatalytic water splitting towards hydrogen production, *Int. J. Hydrogen Energy*, 2019, **44**, 540–577.
- 15 T. C. Jagadale, S. P. Takale, R. S. Sonawane, H. M. Joshi, S. I. Patil, B. B. Kale and S. B. Ogale, N-Doped TiO₂ Nanoparticle Based Visible Light Photocatalyst by Modified Peroxide Sol-Gel Method, *J. Phys. Chem. C*, 2008, **112**, 14595–14602.
- 16 B. Tudu, N. Nalajala, K. P. Reddy, P. Saikia and C. S. Gopinath, Electronic Integration and Thin Film Aspects of Au–Pd/rGO/TiO₂ for Improved Solar Hydrogen, *ACS Appl. Mater. Interfaces*, 2019, **11**, 32869–32878.
- 17 B. Y. Jibril, *React. Kinet* Catalytic performances and correlations with metal oxide band gaps of metal-tungsten mixed oxide catalysts in propane oxydehydrogenation, *Catal. Lett.*, 2005, **86**(1), 171.
- 18 Y.-X. Zhou, Q. Zhang, J.-Y. Gong and S.-H. Yu, Surfactant-Assisted Hydrothermal Synthesis and Magnetic Properties of Urchin-like MnWO₄ Microspheres, *J. Phys. Chem. C*, 2008, **112**, 13383–13389.
- 19 M. Shamshi Hassan, T. Amna, S. S. Al-Deyab, H. Chel Kim and M. Seobkhil, Monodispersed 3D MnWO₄-TiO₂ composite nanoflowers photocatalysts for environmental remediation, *Curr. Appl. Phys.*, 2015, **15**, 753–759.
- 20 R. Lacomba-Perales, D. Errandonea, A. Segura, *et al.*, A combined high-pressure experimental and theoretical study of the electronic band-structure of scheelite-type AWO₄ (A = Ca, Sr, Ba, Pb) compounds, *J. Appl. Phys.*, 2011, 110.
- 21 M. G. Joaquin-Morales, A. F. Fuentes, S. M. Montemayor, M. J. Melendez-Zaragoza, J. M. Salinas Gutierrez, A. Lopezortiz and V. Collins-Martinez, Synthesis conditions effect on the of photocatalytic properties of MnWO₄ for hydrogen production by water splitting, *Int. J. Hydrogen Energy*, 2019, **44**, 12390–12398.
- 22 A. Chakraborty, S. Ganguli and M. A. Kebede, Photocatalytic Degradation of 2-Propanol and Phenol Using Au Loaded MnWO₄ Nanorod Under Visible Light Irradiation, *J. Cluster Sci.*, 2012, **23**, 437–448.
- 23 X. Yan, K. Liu and W. Sh, Facile synthesis of CdS/MnWO₄ heterojunction with enhanced visible-light-driven photocatalytic activity and mechanism investigation, *Colloids Surf., A*, 2017, **520**, 138–145.
- 24 W. S. Choi, K. Taniguchi, S. J. Moon, S. S. A. Seo, T. Arima, H. Hoang, I.-S. Yang, T. W. Noh and Y. S. Lee, Electronic structure and anomalous band-edge absorption feature in multiferroic MnWO₄: an optical spectroscopic study, *Phys. Rev. B: Condens. Matter Mater. Phys.*, 2010, **81**, 205111.
- 25 S. Chen, D. Huang, P. Xu, W. Xue, L. Lei, M. Cheng, R. Wang, X. Liu and R. Deng, Semiconductor-based photocatalysts for photocatalytic and photoelectrochemical water splitting: will we stop with photocorrosion, *J. Mater. Chem. A*, 2020, **8**, 2286–3232.
- 26 J. Jin, J. Yu, D. Guo, C. Cui and W. Ho, A Hierarchical Z-Scheme CdS-WO₃ Photocatalyst with Enhanced CO₂ Reduction Activity, *Small*, 2015, **39**, 5262–5271.
- 27 Y. Liu, Y.-Xiang Yu and W.-D. Zhang, MoS₂/CdS Heterojunction with High Photoelectrochemical Activity for H₂ Evolution under Visible Light: The Role of MoS₂, *J. Phys. Chem. C*, 2013, **117**(25), 12949–12957.
- 28 H. Cui, B. Li, X. Zheng, Y. Zhang, C. Yao, Z. Li, D. Sun and S. Xu, Efficient activity and stability of ZnWO₄/CdS composite towards visible-light photocatalytic H₂ evolution, *J. Photochem. Photobiol., A*, 2019, **384**, 112046.
- 29 L. Zou, H. Wang and X. Wang, High Efficient Photodegradation and Photocatalytic Hydrogen Production of CdS/BiVO₄ Heterostructure through Z-Scheme Process, *ACS Sustainable Chem. Eng.*, 2017, **5**(1), 303–309.



- 30 Y. A. Sethi, R. P. Panmand, S. R. Kadam, A. K. Kulkarni, S. K. Apte, S. D. Naik, N. Munirathnam, M. V. Kulkarni and B. B. Kale, Nanostructured CdS sensitized CdWO₄ nanorods for hydrogen generation from hydrogen sulfide and dye degradation under sunlight, *J. Colloid Interface Sci.*, 2017, **487**, 504–512.
- 31 P. K. Bankar, M. S. Pawar, A. S. Pawbake, S. S. Warule, D. J. Late and M. A. More, Spatially branched CdS–Bi₂S₃ heteroarchitecture: single step hydrothermal synthesis approach with enhanced field emission performance and highly responsive broadband photodetection, *RSC Adv.*, 2016, **6**, 95092–95100.
- 32 Y. Jian-Xi, Z. Gao-ling and H. Gao-rong, The effect of the ratio of thiourea to Cd²⁺ on the properties of CdS nanoparticles, *Microelectron. Eng.*, 2003, **66**, 115.
- 33 S. Dey, R. A. Ricciardo, H. L. Cuthbert and P. M. Woodward, Metal-to-Metal Charge Transfer in AWO₄ (A = Mg, Mn, Co, Ni, Cu, or Zn) Compounds with the Wolframite Structure, *Inorg. Chem.*, 2014, **53**, 4394–4399.
- 34 F. Zhang, Y. Yiu, M. C. Aronson and S. S. Wong, Exploring the room-temperature synthesis and properties of multifunctional doped tungstate nanorods, *J. Phys. Chem. C*, 2008, **112**, 14816–14824.
- 35 M. A. P. Almeida, L. S. Cavalcante, M. S. Li, J. A. Varela and E. Longo, Structural Refinement and Photoluminescence Properties of MnWO₄ Nanorods Obtained by Microwave-Hydrothermal Synthesis, *J. Inorg. Organomet. Polym. Mater.*, 2012, **22**, 264–271.
- 36 M. Nikl, V. V. Laguta and A. Vedda, Complex Oxide Scintillators: Material Defects and Scintillation Performance, *Phys. Status Solidi B*, 2008, **245**, 1701.
- 37 H. Park, W. Choi and M. R. Hoffmann, Effects of the preparation method of the ternary CdS/TiO₂/Pt hybrid photocatalyst on visible light-induced hydrogen production, *J. Mater. Chem.*, 2008, **18**, 2379.
- 38 G. Gouadec and P. Colomban, Raman Spectroscopy of Nanomaterials: How Spectra Relate to Disorder, Particle Size and Mechanical Properties, *Prog. Cryst. Growth Char. Mater.*, 2007, **53**, 1–56.
- 39 G. Gouadecand and P. Colomban, Raman spectroscopy of nanostructures and nanosized materials, *J. Raman Spectrosc.*, 2007, **38**, 598–603.
- 40 K. P. Priyanka, N. Aloysius Sabu, A. T. Sunny, P. A. Sheena and T. Varghese, Effect of Electron Beam Irradiation on Optical Properties of Manganese Tungstate Nanoparticles, *J. Nanotechnol.*, 2013, **2013**, 1–6.
- 41 K. K. Nanda, S. N. Sarangi, S. N. Sahu, S. K. Deb and S. N. Behera, Raman spectroscopy of CdS nanocrystalline semiconductors, *Phys. B Condens. Matter*, 1999, **263**, 31–39.
- 42 P. Gomathisankar, K. Hachisuka, H. Katsumata, T. Suzuki, K. Funasaka and S. Kaneco, Photocatalytic Hydrogen Production from Aqueous Na₂S + Na₂SO₃ Solution with B-Doped ZnO, *ACS Sustainable Chem. Eng.*, 2013, **1**, 982–988.
- 43 M. Chauhan, K. Soni, P. E. Kaethik, K. P. Reddy, C. S. Gopinath and S. Deka, Promising visible-light driven hydrogen production from water on a highly efficient CuCo₂S₄ nanosheet photocatalyst, *J. Mater. Chem. A*, 2019, **7**, 6985–6994.
- 44 R. K. Chava, J. Y. Do and M. Kang, Enhanced photoexcited carrier separation in CdS–SnS₂ heteronanostructures: a new 1D–0D visible-light photocatalytic system for the hydrogen evolution reaction, *J. Mater. Chem. A*, 2019, **7**, 13614.
- 45 S. Guan, X. Fu, Y. Zhang and Z. Peng, β-NiS modified CdS nanowires for photocatalytic H₂ evolution with exceptionally high efficiency, *Chem. Sci.*, 2018, **9**, 1574–1585.
- 46 Y. A. Sethi, R. P. Panmand, A. A. Ambalkar, A. K. Kulkarni, A. Gunjal, D. R. Patil, S. W. Gosavi, M. V. Kulkarni and B. B. Kale, In situ preparation of CdS decorated ZnWO₄ nanorods as a photocatalyst for direct conversion of sunlight into fuel and RhB degradation, *Sustainable Energy Fuels*, 2019, 793–800.
- 47 L. J. Zhang, S. Li, B. K. Liu, D. J. Wang and T. F. Xie, Highly Efficient CdS/WO₃ Photocatalyst: Z-Scheme Photocatalytic Mechanism for Their Enhanced Photocatalytic H₂ Evolution under Visible Light, *ACS Catal.*, 2014, **4**, 3724–3729.

